

1 Revised JVI01749-14

2 **A Chimeric Virus-Mouse Model System for Evaluating the Function and**  
3 **Inhibition of Papain-like Proteases of Emerging Coronaviruses**

4

5 Xufang Deng<sup>a</sup>, Sudhakar Agnihothram<sup>b</sup>, Anna. M. Mielech<sup>a</sup>, Daniel. B. Nichols<sup>a</sup>, Michael. W.  
6 Wilson<sup>c</sup>, Sarah St. John<sup>d</sup>, Scott. D. Larsen<sup>c</sup>, Andrew. D. Mesecar<sup>d</sup>, Deborah. J. Lenschow<sup>e</sup>,  
7 Ralph S. Baric<sup>b</sup> and Susan. C. Baker<sup>a\*</sup>

8

9 <sup>a</sup>Dept of Microbiology and Immunology, Loyola University Chicago Stritch School of Medicine,  
10 Maywood, IL 60153; <sup>b</sup>Depts of Epidemiology and Microbiology and Immunology, University of  
11 North Carolina, Chapel Hill, NC, 27599, <sup>c</sup>Vahlteich Medicinal Chemistry Core, College of  
12 Pharmacy, University of Michigan, Ann Arbor, MI 48109; <sup>d</sup>Depts of Biological Science and  
13 Chemistry, Purdue University, West Lafayette, IN 47907; <sup>e</sup>Dept of Internal Medicine & Dept of  
14 Pathology and Immunology, Washington University School of Medicine, St. Louis, MO 63110

15

16 **Running title:** Chimeric virus to evaluate CoV PLpro inhibitors

17

18 \*Corresponding author: Susan C. Baker, PhD, E-mail: [sbaker1@luc.edu](mailto:sbaker1@luc.edu)

19 Word count: Abstract (249); Importance (120); Text (4611)

20 **Abstract**

21 To combat emerging coronaviruses, developing safe and efficient platforms to evaluate viral  
22 protease activities and the efficacy of protease inhibitors is a high priority. Here we exploit a  
23 biosafety level 2 (BSL-2) chimeric Sindbis virus system to evaluate protease activities and the  
24 efficacy of inhibitors directed against the papain-like protease (PLpro) of Severe Acute  
25 Respiratory Syndrome coronavirus (SARS-CoV), a biosafety level 3 (BSL-3) pathogen. We  
26 engineered Sindbis virus to co-express PLpro and a substrate, murine interferon stimulated  
27 gene 15 (ISG15), and found that PLpro mediates removal of ISG15 (deISGylation) from  
28 cellular proteins. Mutation of the catalytic cysteine residue of PLpro or addition of a PLpro  
29 inhibitor blocked deISGylation in virus-infected cells. Thus, deISGylation is a marker of PLpro  
30 activity. Infection of Interferon-alpha/beta receptor knockout (IFNAR<sup>-/-</sup>) mice with these  
31 chimeric viruses revealed that PLpro deISGylation activity removed the ISG15-mediated  
32 protection during viral infection. Importantly, administration of a PLpro inhibitor protected  
33 these mice from lethal infection demonstrating the efficacy of a coronavirus protease inhibitor  
34 in a mouse model. However, this PLpro inhibitor was not sufficient to protect mice from lethal  
35 infection with SARS-CoV MA15, suggesting that further optimization of the delivery and  
36 stability of PLpro inhibitors is needed. We extended the chimeric virus platform to evaluate  
37 papain-like protease/deISGylating activity of Middle East Respiratory Syndrome Coronavirus  
38 (MERS-CoV), to provide a small animal model to evaluate PLpro protease inhibitors to this  
39 recently emerged pathogen. This platform has the potential to be universally adaptable to  
40 other viral and cellular enzymes that have deISGylating activity.

41 **Importance**

42 Evaluating viral protease inhibitors in a small animal model is a critical step in the pathway  
43 toward antiviral drug development. We modified a biosafety level 2 chimeric virus system to  
44 facilitate evaluation of inhibitors directed against highly pathogenic coronaviruses. We used  
45 this system to demonstrate the *in vivo* efficacy of an inhibitor of the papain-like protease of  
46 Severe Acute Respiratory Syndrome Coronavirus. Furthermore, we demonstrate that the  
47 chimeric virus system can be adapted to study the proteases of emerging human pathogens  
48 such as Middle East Respiratory Syndrome Coronavirus. This system provides an important  
49 tool to rapidly assess the efficacy of protease inhibitors targeting existing and emerging  
50 human pathogens as well as other enzymes capable of removing ISG15 from cellular  
51 proteins.

52 **Introduction**

53 Emerging coronaviruses (CoVs) are now recognized for their life-threatening potential.  
54 The outbreak of Severe Acute Respiratory Syndrome coronavirus (SARS-CoV) that occurred  
55 a decade ago resulted in over 8000 infected people with 10% mortality (1). A recently  
56 emerged coronavirus, designated Middle East Respiratory Syndrome coronavirus  
57 (MERS-CoV), has infected over 837 people, with 291 deaths as of July 24, 2014 (2).  
58 Epidemiologic studies implicate animal reservoirs as the source for emerging coronaviruses.  
59 By identifying a SARS-like CoV from Chinese horseshoe bats and analyzing the mutations in  
60 the spike glycoprotein, first in intermediate hosts and then in humans, researchers were able  
61 to document the evolution of an emerging CoV (3). The footprint for the evolution of  
62 MERS-CoV is not yet clear. MERS-CoV has about 80% genome sequence identity to the bat  
63 coronaviruses HKU4 and HKU5 (4, 5). In addition, infectious MERS-CoV has been isolated  
64 from the respiratory tract of young camels (6–8) and there is accumulating evidence that adult  
65 camels have specific antibodies to MERS-CoV, consistent with endemic infection in the camel  
66 population (9, 10). Currently, it is unclear if the human cases of MERS are from sporadic  
67 introduction from animal reservoirs with limited human to human transmission or if there is  
68 ongoing transmission of MERS-CoV in asymptomatic humans or intermediate hosts (11–13).  
69 It is clear that CoVs have zoonotic potential for crossing the species-barrier and emerging into  
70 the human population to cause lethal disease.

71 Viral proteases are logical targets for antiviral drug development, and protease inhibitors  
72 have been identified to block the papain-like protease (PLpro) domain of SARS-CoV (14).

73 PLpro is encoded in the viral replicase polyprotein and is critical for processing the polyprotein  
74 to generate a functional replicase complex. Structural and enzymatic studies revealed that  
75 PLpro is also a viral deubiquitinase (DUB), which can cleave ubiquitin (Ub) or ubiquitin-like  
76 molecules, such as interferon stimulated gene 15 (ISG15), from substrate proteins (15–17).  
77 Moreover, the catalysis-dependent interferon antagonism of PLpro implies that it may be  
78 involved in evading host innate immunity (18, 19). High-throughput screening efforts led to the  
79 identification of small molecule inhibitors directed against the viral papain-like protease  
80 domain, and synthetic medicinal chemistry and structure-activity relationship studies have  
81 produced compounds that inhibit replication of SARS-CoV in cell culture (14, 20). However,  
82 one of the challenges for preclinical, antiviral drug development is the availability of a small  
83 animal model for emerging CoVs. For SARS-CoV, infection of mouse-adapted strains in mice  
84 (21, 22) or transgenic mice expressing the receptor (Angiotensin-converting enzyme 2, ACE2)  
85 (23, 24), may serve as model systems for evaluating the efficacy of therapeutics. However,  
86 these studies must be performed in biosafety level 3 laboratories (BSL-3) with select agent  
87 status. For MERS-CoV, although rhesus macaques can be infected (25, 26), less expensive  
88 animal models such as mice and hamster are not susceptible to natural infection (27, 28).  
89 Dipeptidyl peptidase 4 (DPP4) was identified as the receptor for MERS-CoV in human and bat  
90 cells (29). Recently, novel model systems were generated for MERS-CoV infection by  
91 infecting mice with recombinant adenovirus expressing the human DPP4 receptor, which  
92 renders them susceptible to infection under BSL-3 conditions (30) and by generating  
93 recombinant HKU5-expressing the SARS-CoV spike protein (31). Development of additional

94 affordable and adaptable small animal models is needed to evaluate antivirals against  
95 existing and potentially emerging coronaviruses.

96       The goal of our study was to develop a biosafety level 2 system to evaluate inhibitors of  
97 the papain-like proteases of highly pathogenic emerging coronaviruses such as SARS-CoV  
98 and MERS-CoV. We were inspired by the fundamental work of Frias-Stahli et al., who first  
99 demonstrated that a chimeric Sindbis virus system could be used to evaluate the potential  
100 protease activity of a BSL-4 pathogen, Crimean Congo Hemorrhagic Fever virus (36). This  
101 chimeric virus system is based on the use of the positive-strand RNA virus, Sindbis virus (SV),  
102 a BSL-2 pathogen that is rapidly cleared by the immune system after infection in mice.  
103 Lenschow and co-workers showed that the interferon response, particularly interferon  
104 stimulated gene 15 (ISG15), is critical for efficient clearance of SV (35). Consequently, SV  
105 infection of interferon receptor knockout mice ( $IFNR^{-/-}$ ), which are unable to signal the  
106 induction of interferon stimulated genes, results in a lethal infection. However, if the gene for  
107 ISG15 is inserted into and expressed by SV, then infection with the chimeric virus induces an  
108 antiviral state and mice are protected from lethal infection. To induce the antiviral state,  
109 ISG15 must be conjugated to host cell proteins, a process termed ISGylation (40). The  
110 removal of ISG15 by deISGylating enzymes such as the L protease of CCHFV results in the  
111 abrogation of the protection mediated by ISG15 and mice succumb to infection. Thus,  
112 deISGylating enzymes can be used to “toggle off” the effect of ISG15 in this system. Given  
113 that the PLpros of CoVs not only function to process the viral polyprotein but also possess  
114 deISGylating activity (15, 37), we reasoned that the chimeric Sindbis-ISG15-Protease (SIP)

115 system could be exploited as a surrogate system to evaluate enzymatic activity and inhibition  
116 of CoV PLpros. Here we demonstrate the utility of the chimeric SIP system for evaluating the  
117 deISGylating activities of PLpros from SARS-CoV and MERS-CoV and the efficacy of a  
118 SARS-CoV PLpro inhibitor.

119

## 120 **Materials and Methods**

121 **Cells, virus and plasmids.** Baby hamster kidney cell line (BHK-21) and Vero-E6 cells were  
122 cultured in Dulbecco's modified Eagle's medium containing 10% (vol/vol) fetal calf serum  
123 (FCS), supplemented with penicillin (100 U/ml) and streptomycin (100µg/ml). Stocks of the  
124 recombinant mouse-adapted SARS-CoV (rMA15) were propagated and titrated on Vero-E6  
125 cells. The virus was cryopreserved at -80°C until use as described below.  
126 PcDNA3-6×myc-mISG15 was kindly provided by Min-Jung Kim (Pohang University of  
127 Science and Technology, Pohang, Republic of Korea). PcDNA3-Ube1L, pcDNA3-UbcH8 and  
128 pcDNA3-Herc5 were kind gifts from Robert M. Krug (University of Texas).  
129 pcDNA-MERS-PLpro and its catalytic mutant (C1592A) were generated in our lab as  
130 described (38).

131 **PLpro inhibitors 3e and 3h.** The synthesis and characterization of these inhibitors were  
132 described in Baez-Santos et al (39). For mice administration, inhibitor 3e was formulated with  
133 5% DMSO, 25% polyethylene glycol (PEG400) and 70% PBS (vol/vol/vol).

134 **SIP viruses.** The Sindbis virus vector, dsTE12Q, was kindly provided by Dr. Deborah  
135 Lenschow (Washington University in St. Louis). To generate the chimeric Sindbis virus

136 expressing ISG15 and PLpro, the DNA fragment of ISG15-IRES-PLpro comprising the murine  
137 ISG15 cDNA (1~465 nt), hepatitis C virus internal ribosome entry site (HCV-IRES: 40-371nt of  
138 genome of HCV 2b genotype), and PLpro in frame with a V5 epitope tag at the C-terminus  
139 (available upon request), were generated by synthesis or two-step overlapping PCR and  
140 subsequently cloned into the BstE II restriction site of dsTE12Q vector. The insert DNAs of  
141 each chimeric virus were generated as follows:

142 **1) SIP-SWT and SIP-SMT.** A DNA sequence comprising the ISG15-IRES-PLpro (amino  
143 acids1599-1855 in pp1a of SARS-CoV, accession number AY278241) in frame with V5  
144 epitope tag was codon-optimized, synthesized, and subcloned into the pUC57 vector  
145 (Genscript, NJ). A catalytically inactive mutant of PLpro (cysteine 1651 to alanine) was  
146 generated as described previously (19) by site-directed mutagenesis PCR using primers  
147 (available upon request).The DNAs of interest were cut from recombinant pUC57 plasmids  
148 and cloned into the TE12Q vector, and designated SIP-SWT and SIP-SMT, respectively.

149 **2) SIP-MWT and SIP-MMT.** A DNA sequence comprising of ISG15-IRES-PLpro (amino  
150 acids1483-1802 in pp1a of MERS-CoV, accession number AFS88944) was generated by  
151 two-step overlapping PCR using primers (available upon request).Briefly, the fragment of  
152 ISG15-IRES was amplified from the recombinant pUC57 plasmid described above, and the  
153 fragment of MERS-CoV PLpro or its catalytic mutant in frame with V5 epitope was amplified  
154 from the plasmids of pcDNA-MERS-PLpro or its catalytic mutant (cysteine 1592 to alanine),  
155 respectively. The fragment of ISG15-IRES-PLpro was generated by PCR amplification using  
156 primers (available upon request) and cloned into the BstE II restriction site of the TE12Q



157 vector, and designated SIP-MWT and SIP-MMT, respectively.

158 All constructs were verified by sequencing and linearized by digestion with *Xho* I  
159 restriction enzyme. The viral RNA was synthesized by *in vitro* transcription reaction following  
160 the manufacturer's instructions (Ambion) and the RNA was subsequently electroporated into  
161 the BHK-21 cells with 3 pulses at conditions of 850V, 25 $\mu$ F in a 0.4cm cuvette cap (Bio-Rad).  
162 Viral supernatants were harvested at 16~24 hours (hrs) post electroporation and the titers  
163 were determined by standard plaque assay on the BHK-21 cells.

164 **Western blotting.** Cell lysates were separated in a 10% SDS-PAGE gel and transferred to  
165 PVDF membrane in transfer buffer (25mM Tris, 192mM glycine, 20% methanol) for 1 hr at  
166 65V. The membrane was blocked using 5% dried skim milk in TBST buffer (0.9% NaCl, 10mM  
167 Tris-HCl, pH7.5, 0.1% Tween 20) for 2 hrs at room temperature and subsequently incubated  
168 with primary antibodies for overnight at 4°C. The mouse anti-myc tag monoclonal antibody  
169 (MBL) was used to detect the myc-ISG15 and the ISGylated proteins. ISG15 was detected  
170 using rabbit anti-ISG15 polyclonal antibodies (kind gift of the Lenschow lab). The expression  
171 of PLpro and  $\beta$ -actin were detected using mouse anti-V5 (Invitrogen) and anti-beta actin  
172 (Ambion) monoclonal antibodies, respectively. HRP-conjugated goat-anti mouse (Southern  
173 Biotech) was used as the secondary antibody and detected by using Western Lighting  
174 Chemiluminescence Reagent Plus (PerkinElmer) and visualized using a FluoroChem E  
175 Imager.

176 **Viral growth kinetics.** To analyze the replication of SIP viruses, the viral growth kinetics  
177 assays were performed. Briefly, 10<sup>5</sup> BHK-21 cells per well in 24-well plate were infected with

178 each SIP virus at a multiplicity of infection (MOI) of 5 and the cell supernatants were collected  
179 at indicated time points. The viral titers of the supernatants were determined by standard  
180 plaque assay on the BHK-21 cells.

181 **DeISGylation assay.** To determine the deISGylating activity of PLpro, BHK-21 cells in 24-well  
182 plate were transfected with 0.25 µg pcDNA3-myc-ISG15 and 0.125 µg each of ISGylating  
183 enzymes expression plasmids (pcDNA3-Ube1L, pcDNA3-UbcH8, and pcDNA3-Herc5) by  
184 Lipofectamine 2000 following the manufacturer's instructions. At 6 hrs post-transfection, the  
185 medium was removed and replaced by mock or viral inoculums of SIP virus at MOI of 5. After  
186 1 hr inoculation at 37°C, the inoculums were replaced by fresh DMEM containing 1% FCS.  
187 Cell lysates were prepared at 18 hrs post infection using 100 µL lysis buffer [4% SDS, 3%  
188 dithiothreitol (DTT), and 65mM Tris, pH 6.8] and analyzed by Western blotting.

189 To determine the effect of PLpro inhibitors on the deISGylating activity, BHK-21 cells  
190 were subjected to transfection and infection as described above, followed by the addition of  
191 fresh 1% FCS DMEM media containing the inhibitor at final concentration of 50 µM or a serial  
192 dilution. After 17 hrs of treatment (18 hrs post infection), cell lysates were prepared and  
193 analyzed by western blotting as described above.

194 **Infection of mice with SIP viruses.** Type 1 Interferon receptors knockout (IFNAR<sup>-/-</sup>) mice on  
195 the C57BL/6 background were initially obtained from Dr. Deborah Lenschow (Washington  
196 University in St. Louis). Mice were bred and maintained at Loyola University Chicago in  
197 accordance with all federal and university guidelines. Seven to eight-week-old male IFNAR<sup>-/-</sup>  
198 mice were infected subcutaneously in the left hind footpad with 6×10<sup>6</sup> PFU of SIP virus diluted

199 in 25  $\mu$ L DMEM medium followed by daily body weight monitoring. When the weight loss of an  
200 infected mouse was more than 25% of the initial body weight, the mouse was humanely  
201 euthanized. The survival rate was calculated by counting the dead or euthanized mice  
202 number and analyzed by log-rank test with GraphPad Prism software.

203 To determine if the PLpro inhibitor can block the function of PLpro *in vivo*, we tested  
204 PLpro 3e inhibitor in mice infected with SIP viruses. For each injection, 50  $\mu$ g per dose of  
205 administered intraperitoneally (i.p.) at 0 and 2 day post infection (d.p.i). The weight loss of  
206 mice was monitored daily and survival rate was analyzed as described above.

207 **Infection of mice with SARS-CoV MA15 virus.** All viral and animal experiments were  
208 performed in a class II biological safety cabinet in a certified biosafety level 3 laboratory  
209 containing redundant exhaust fans, and workers wore personnel protective equipment,  
210 including Tyvek suits, hoods, and high-efficiency particle arrestor-filtered powered  
211 air-purifying respirators (PAPRs).

212 Eight-week old BALB/c mice were purchased from Harlan Laboratories and housed in  
213 accordance with all UNC-Chapel Hill Institutional Animal Care and Use Committee (IACUC)  
214 guidelines. Mice were administered either intranasally (i.n.) a single dose of 20  $\mu$ g Poly (I:C),  
215 or i.p. 50  $\mu$ g per dose of inhibitor 3e or vehicle. Mice were anesthetized with a mixture of  
216 ketamine-xylazine and were infected i.n. either with the  $2 \times 10^4$  PFU rMA15 virus or with  
217 phosphate-buffered saline (PBS) in a dose of 50  $\mu$ L. Infected animals were monitored daily for  
218 weight loss and sacrificed upon approaching 80% of their starting body weight or manifesting  
219 severe clinical symptoms, according to the IACUC guidelines. The lung tissues of infected

220 mice were collected at 4 d.p.i. and the viral titers were determined by plaque assay on  
221 Vero-E6 cells.

## 222 **Results**

223 **Exploiting Chimeric Sindbis virus to evaluate CoV PLpro activity.** The goal of our study  
224 was to establish a BSL-2 mouse model system to assess the function of CoV PLpros and to  
225 evaluate PLpro inhibitors *in vivo*. To do this, we modified a chimeric Sindbis virus that  
226 co-expresses ISG15 and a viral OTU domain deISGylating enzyme (36). To modify the  
227 system to allow expression of the larger Ubiquitin Specific Protease (USP) family enzyme  
228 from SARS-CoV, we replaced the original EMCV IRES with the IRES from HCV. A dicistronic  
229 DNA fragment containing ISG15 cDNA followed by the HCV-IRES and subsequent PLpro  
230 coding region was synthesized and inserted into the BstE II site of recombinant Sindbis  
231 genome, namely Sindbis-ISG15-IRES-PLpro (SIP). Four chimeric Sindbis viruses expressing  
232 either wild-type (WT) or catalytic cysteine mutant PLpros (MT) from SARS-CoV and  
233 MERS-CoV were generated, and named as SIP-SWT, SIP-SMT, SIP-MWT, and SIP-MMT,  
234 respectively (Fig. 1A). The expression of ISG15 and PLpro was detected by immunoblotting  
235 lysates prepared from virus-infected cells (Fig. 1B). Analysis of viral growth kinetics revealed  
236 that the four SIP viruses replicate with similar kinetics and to high titer in BHK-21 cells (Fig.  
237 1C). Furthermore, these viruses were stable upon passage in BHK-21 cells, which was in  
238 contrast to chimeric viruses containing larger insertions that had an EMCV IRES (Data not  
239 shown).

240 **PLpros expressed by chimeric Sindbis virus have deISGylating activity.** To determine  
241 whether PLpros expressed from Sindbis virus is able to cleave ISG15, BHK-21 cells were  
242 transfected with plasmids expressing ISGylation substrates and enzymes (myc tagged ISG15,  
243 Ube1L, UbcH8, and Herc5) and subsequently infected with SIP-WT or SIP-MT viruses.  
244 Western blot results show that cellular proteins were ISGylated in mock-infected cells  
245 transfected with ISGylation machinery plasmids. In contrast, the level of ISGylated proteins  
246 was significantly reduced in cells infected with SIP-WT but not SIP-MT viruses (Fig.2). The  
247 decreased level of ISGylated proteins in SIP-WT infected cells is not due to virus induced cell  
248 death or lack of host translation in the context of a Sindbis virus infection as the SIP-MT grows  
249 to similar levels as the SIP-WT (Fig. 1C), and cellular proteins are ISGylated in SIP-MT  
250 infected cells. These results indicate that both SARS-CoV PLpro and MERS-CoV PLpro  
251 exhibit broad deISGylating activity, even when expressed in the context of Sindbis virus  
252 infection. These results extend the work of Frias-Staheli et al. (36) and show that viral  
253 USP-type enzymes, like the viral OTU-type enzyme used in their study, can function as  
254 deISGylating proteases in the context of Sindbis virus infection.

255 **PLpro disrupts ISG15-mediated protection in mice.** To determine whether co-expression  
256 of PLpro removes the protective effect of ISG15 during Sindbis virus infection, we infected  
257 IFNAR<sup>-/-</sup> mice with the SIP-SWT or SIP-SMT and monitored for weight loss and survival. Mice  
258 exhibiting greater than 25% weight loss were humanely euthanized in accordance with animal  
259 care guidelines. As expected, the mice infected with SIP-SWT virus lost more body weight

260 than mice infected with SIP-SMT virus at day 2~5 post infection (d.p.i) (Fig. 3A). SIP-SWT  
261 infection results in over 80% mortality, which is significantly higher than the mortality observed  
262 in mice infected with the SIP-SMT virus (26.7%) (P=0.0005; Fig. 3B). Moreover, we found the  
263 SIP virus expressing wild-type PLpro from MERS-CoV (SIP-MWT), but not catalytic inactive  
264 cysteine mutant of MERS-CoV PLpro (SIP-MMT) is able to inhibit the ISG15 function. The  
265 weight loss at 4~5 d.p.i and the mortality of mice infected with SIP-MWT were significant more  
266 than those of SIP-MMT infected-mice (Fig. 3C and 3D). These results indicate that PLpros of  
267 SARS-CoV and MERS-CoV are capable of disrupting the ISG15-mediated protection in  
268 IFNAR<sup>-/-</sup> mice, suggesting its role in antagonizing the innate immune response. In our system,  
269 the SIP virus infected-mice approached the maximum weight loss at 5~6 d.p.i and then either  
270 recovered or succumbed to infection, whereas in Frias-Staheli's work the majority of chimeric  
271 virus infected-mice succumbed to infection at 8~12 d.p.i. The differential survival time may  
272 due to the different genetic background of mouse strains (129/SV/Pas in their work) or the  
273 expressions of different proteases. Next, we wanted to determine if this chimeric  
274 Sindbis-mouse system could be used for evaluating small molecule inhibitors directed against  
275 the PLpro domain.

276 **An Inhibitor of SARS-CoV PLpro specifically blocks deISGylating activity.** We reported  
277 the identification of small molecule compounds that block PLpro activity *in vitro* and block the  
278 replication of SARS-CoV in cell culture (14, 20). We recently designed and evaluated the  
279 biological activity of a second-generation of SARS-CoV PLpro inhibitors *in vitro* (39). One of

280 these compounds, 3e, inhibits SARS-CoV PLpro with a potency of 390 nM and has an  
281 antiviral potency of 8.3  $\mu$ M against SARS-CoV in Vero-E6 cells. Importantly, this compound is  
282 not cytotoxic, does not bind to human serum albumin and has increased metabolic stability  
283 compared to other compounds evaluated (39). Therefore, to determine if compound 3e  
284 blocked PLpro activity in the context of the chimeric SIP virus, we exploited the deISGylation  
285 assay in cell culture. We found that the cells treated with compound 3e, but not the control  
286 compound 3h (Fig. 4A), a structural homolog of 3e with a higher  $IC_{50}$  (600 nM) and no antiviral  
287 activity (39), showed an increase in the level of ISGylated proteins in SIP-WT virus-infected  
288 cells (Fig. 4B). This indicates that the deISGylating activity of PLpro was blocked by  
289 compound 3e. We also found that the deISGylating activity of PLpro was inhibited by  
290 compound 3e in a dose-dependent manner (data not shown). To assess the specificity of  
291 compound 3e, we tested the activity of a cellular deISGylating enzyme USP18 (also known as  
292 Ubp43) in the presence of 3e. Western blot results revealed that the level of ISGylated  
293 proteins in USP18-transfected cells was significantly decreased compared to the control; and  
294 there was no observable change in level of ISGylation in the transfected cells treated with  
295 compound 3e (Fig. 4C). This result indicates that compound 3e does not inhibit the  
296 deISGylating activity of USP18. Taken together, these results suggest that compound 3e  
297 specifically blocks SARS-CoV PLpro deISGylating activity in cell culture during replication of  
298 the SIP virus.

299 **SARS-CoV PLpro protease inhibitor 3e protects mice from lethal SIP virus infection.** To

300 determine whether the PLpro inhibitor was effective in a small animal model, we injected  
301 IFNAR<sup>-/-</sup> mice subcutaneously with SIP-WT and administered intraperitoneally (i.p.)  
302 compound 3e (50µg/dose) at 0 and 2 d.p.i. Although we found there is no significant weight  
303 loss between 3e and vehicle treated mice at early time points except at 5 d.p.i. (P<0.01), the  
304 majority of the 3e treated-mice (64.7%) recovered from infection before approaching the  
305 weight loss of euthanasia. In contrast, SIP-WT infected mice administered the vehicle control  
306 exhibited significantly higher mortality (31.6% survival rate, P=0.021; Fig. 5). The effect of  
307 compound 3e was specific to SARS-CoV PLpro activity as it had no significant effect on the  
308 pathogenesis of Sindbis virus infection of IFNAR<sup>-/-</sup> mice and there was no evidence of weight  
309 loss in mice injected with the compound 3e alone (data not shown). These results  
310 demonstrate the protective effect of compound 3e during SIP-WT virus infection.

311 **Evaluation of inhibitor 3e in SARS-CoV MA15 infected-mice.** To extend our studies to a  
312 respiratory tract model system, we evaluated 3e using the established SARS-CoV-MA15  
313 intranasal infection model (21). Wild-type Balb/c mice were pretreated intranasally with 20µg  
314 single dose of Poly (I:C) as a positive control or 1 dose of compound 3e (50µg/dose) at 4 h  
315 prior to infection. Over all, mice were administered 50µg/dose of 3e twice a day on Day 0 (4h  
316 post infection), 1 and 2 post infection, and the mice were monitored for weight loss through  
317 day 4 post infection, and virus titers in lungs were assessed on day 4 post infection. Mice  
318 treated with compound 3e were not protected from virus induced weight loss, or virus  
319 replication, whereas the Poly (I:C) treated mice were completely protected from weight loss,



320 and the virus titers on Day 4 showed significant reduction in virus replication, compared to  
321 untreated virus control (Fig. 6). The results suggest that although protease inhibitor 3e was  
322 capable of protecting the majority of mice from lethal systemic SIP virus infection, the inhibitor  
323 is either not sufficiently stable or bioavailable in the respiratory tract to reduce the replication  
324 and pathogenesis of a respiratory tract infection with SARS-CoV MA15 in mice.

### 325 **Discussion**

326 This work establishes a chimeric Sindbis virus-mouse model system for assessing  
327 deISGylating activity of SARS-CoV and MERS-CoV PLpros and for evaluating SARS-CoV  
328 PLpro inhibitors in BSL-2 containment. To develop this model system, we exploited a chimeric  
329 Sindbis system pioneered by Frias-Staheli and coworkers who first showed that viral  
330 proteases with deISGylating activity could remove the protective antiviral state induced by  
331 ISG15 (36). We extended their studies by: 1) modifying the chimeric virus to express either  
332 SARS-CoV PLpro or MERS-CoV PLpro under translational control of the HCV-IRES, this  
333 shortened IRES enabled insertion of larger CoV USP-like proteases; and 2) showing that  
334 SARS-CoV PLpro inhibitors could be evaluated in SIP virus-infected IFNAR<sup>-/-</sup> mice. This is the  
335 first demonstration of the efficacy and specificity of an inhibitor that targets a viral papain-like  
336 cysteine protease (PLpro) in a virus-infected animal. This is important because there are over  
337 100 cellular DUBs and previously it was unclear if the PLpro inhibitor was sufficiently specific  
338 to alter protease/deISGylating activity in an infected animal. In general, this chimeric  
339 Sindbis-protease system enables the study of enzymes with deISGylating activity, and

340 establishes a BSL-2 model that can be used to evaluate the efficacy of small molecule  
341 inhibitors to existing and emerging coronaviruses *in vivo*.

342 We hypothesize that the multifunctionality of CoV PLpros as proteases, deubiquitinating  
343 and deISGylating enzymes is important in viral pathogenesis, especially in antagonizing the  
344 innate immune response. ISG15 functions as an antiviral molecule through ISGylation of host  
345 substrates and by eliciting cytokine activity (39). Mice lacking ISG15 are more susceptible to  
346 lethal infection with Sindbis virus, herpesvirus and influenza virus (35, 41). The role of ISG15  
347 in CoV pathogenesis is not yet clear. Ma and co-workers showed that murine coronavirus  
348 infection of USP18-deficient mice, where ISGylation levels are high, resulted in lower viral  
349 titers and prolonged survival compared to wild type mice, suggesting that high levels of  
350 ISGylation may delay CoV replication and pathogenesis (42). However, USP18 also mediates  
351 ISGylation-independent dendritic cells maturation (43), thus the loss of USP18 function may  
352 affect the kinetics of the immune response to viral infection. In the present study, we directly  
353 shown that CoV PLpros are capable of disrupting the protective effect of ISG15 *in vivo*,  
354 suggesting that PLpros have evolved an ISGylation antagonism mechanism to promote viral  
355 replication.

356 A major advantage of the SIP virus system is that we were able to study the PLpros of  
357 pathogenic CoVs in mice in a BSL-2 environment. This is particularly important because of  
358 the limited number of small animal models currently available for the study of MERS-CoV  
359 PLpro inhibitors (30, 31). MERS-CoV enters cells by interaction with DPP4 and both human  
360 and bat DPP4 are functional receptors (29). In contrast, mice and rats are resistant to

361 infection (27, 28), likely because of differences in the portion of DPP4 that interacts with the  
362 receptor binding domain of the spike glycoprotein of MERS-CoV (44, 45). The development of  
363 mouse-adapted strains of MERS-CoV and the generation of transgenic mice expressing the  
364 human DPP4 receptor are aimed at providing critical tools needed for understanding  
365 pathogenesis and evaluating candidate vaccines, but this work will be performed in BSL-3  
366 containment. In contrast, the SIP virus mouse model is used in BSL-2 containment, and  
367 experiments are cost effective for evaluating efficacy and toxicity of PLpro inhibitors. In  
368 addition, we envision expanding the SIP virus system to identify broad spectrum PLpro  
369 inhibitors that block a wide array of human and bat PLpro activity and protect mice from lethal  
370 viral infection. Using the SIP system, we can evaluate the efficacy of an inhibitor to a novel bat  
371 PLpro without the need for developing a transgenic mouse model expressing the receptor for  
372 the novel virus. An important caveat of the SIP virus system is that it is a systemic infection  
373 and lethality is due to transmission of the virus through the central nervous system (35). Thus,  
374 it is a very sensitive system for evaluating protease inhibitors and we demonstrate efficacy of  
375 protease inhibitor 3e, which was previously shown to block replication of SARS-CoV in cell  
376 culture (39). However, as we report here, protease inhibitors must also be evaluated in the  
377 context of a respiratory tract infection, such as with mouse adapted-SARS-CoV-MA15 (21,  
378 22). We found that protease inhibitor 3e was not effective at blocking replication and  
379 pathogenesis of SARS-CoV-MA15 in the respiratory tract of infected mice. This lack of  
380 efficacy may be due to the relative instability of 3e (39), or limitations of delivery into the  
381 mucosal surfaces of the respiratory tract, the site of natural infection. Further work is required

382 to optimize PLpro inhibitors for bioavailability, stability and appropriate delivery to block  
383 replication and pathogenesis of coronavirus.

384       Papain-like proteases (PLpros or PLPs) are conserved in all coronaviruses and the goal  
385 of identifying a broad spectrum inhibitor would be to inhibit existing human and potential  
386 emerging CoVs. Several CoV PLPs have been identified as deISGylating enzymes, such as  
387 the PLpro domain of SARS-CoV (15) and the PLP2 domain of human coronavirus NL63  
388 (HCoV-NL63) (19). The SIP system described here could be extended to study the function of  
389 the PLpro/PLP2 domain of endemic human coronaviruses such as HCoV-NL63, HCoV-HKU1,  
390 HCoV-229E and HCoV-OC43. HCoV-NL63 generally causes mild upper respiratory disease in  
391 adult but it can cause more severe respiratory disease in young children (46, 47).  
392 HCoV-HKU1 has been associated with pneumonia in the elderly (48). Currently there are no  
393 animal models for evaluating inhibitors to HCoV-NL63 or HCoV-HKU1. Other PLPs including  
394 those of bat coronaviruses are speculated to act as deISGylating enzymes as well since they  
395 share conserved catalytic elements and are predicted to recognize similar cleavage sites in  
396 the viral polyprotein. We are currently developing SIP viruses expressing the PLP2 domain of  
397 HCoV-NL63 and other CoVs with the long term goal of identifying broad spectrum PLpro  
398 inhibitors that could block replication of existing and emerging coronaviruses.

399 Overall, this study provides evidence of CoV PLpro deISGylating activity in the context of viral  
400 infection and establishes a BSL-2 animal model for evaluating PLpro inhibitors in a mouse  
401 model. The current studies are designed to facilitate antiviral drug development for existing

402 and emerging coronavirus infections and are a forerunner to the development of similar  
403 platforms aimed at testing inhibitors against other delSGylating enzymes *in vivo*.

404 **Acknowledgments**

405 We thank Jonathan E. Snyder and Dr. Richard Kuhn at Purdue University for providing  
406 reagents. We thank Dr. Tom Gallagher at Loyola University Chicago for his helpful comments  
407 on the manuscript. We also thank Andy Kilianski in the Baker lab for his technical support and  
408 discussions.

409 This work was supported by the National Institutes of Health (NIAID-R01AI085089 to  
410 S.C.B. and A.D.M.) and NIAID U19 AI 107810 to R.S.B. A.M.M was supported by an Arthur J.  
411 Schmitt fellowship (Loyola University Chicago).

412 **References**

- 413 1. **Perlman S, Netland J.** 2009. Coronaviruses post-SARS: update on replication and  
 414 pathogenesis. *Nat. Rev. Microbiol.* **7**:439–50.
- 415 2. **World Health Organization (WHO):** Global Alert and Response. Available at  
 416 [http://www.who.int/csr/don/2014\\_06\\_23\\_mers/en/](http://www.who.int/csr/don/2014_06_23_mers/en/). Accessed at July 24, 2014
- 417 3. **Song H-D, Tu C-C, Zhang G-W, Wang S-Y, Zheng K, Lei L-C, Chen Q-X, Gao Y-W,**  
 418 **Zhou H-Q, Xiang H, Zheng H-J, Chern S-WW, Cheng F, Pan C-M, Xuan H, Chen S-J,**  
 419 **Luo H-M, Zhou D-H, Liu Y-F, He J-F, Qin P-Z, Li L-H, Ren Y-Q, Liang W-J, Yu Y-D,**  
 420 **Anderson L, Wang M, Xu R-H, Wu X-W, Zheng H-Y, Chen J-D, Liang G, Gao Y, Liao M,**  
 421 **Fang L, Jiang L-Y, Li H, Chen F, Di B, He L-J, Lin J-Y, Tong S, Kong X, Du L, Hao P,**  
 422 **Tang H, Bernini A, Yu X-J, Spiga O, Guo Z-M, Pan H-Y, He W-Z, Manuguerra J-C,**  
 423 **Fontanet A, Danchin A, Niccolai N, Li Y-X, Wu C-I, Zhao G-P.** 2005. Cross-host  
 424 evolution of severe acute respiratory syndrome coronavirus in palm civet and human. *Proc.*  
 425 *Natl. Acad. Sci. U. S. A.* **102**:2430–5.
- 426 4. **Zaki AM, van Boheemen S, Bestebroer TM, Osterhaus ADME, Fouchier R a M.** 2012.  
 427 Isolation of a novel coronavirus from a man with pneumonia in Saudi Arabia. *N. Engl. J.*  
 428 *Med.* **367**:1814–20.

- 429 5. **Van Boheemen S, de Graaf M, Lauber C, Bestebroer TM, Raj VS, Zaki AM, Osterhaus**  
 430 **ADME, Haagmans BL, Gorbalenya AE, Snijder EJ, Fouchier RAM.** 2012. Genomic  
 431 characterization of a newly discovered coronavirus associated with acute respiratory  
 432 distress syndrome in humans. *MBio* **3**:e00473–12.
- 433 6. **Memish ZA, Cotten M, Meyer B, Watson SJ, Alshafi AJ, Al Rabeeah AA, Corman VM,**  
 434 **Sieberg A, Makhdoom HQ, Assiri A, Al Masri M, Aldabbagh S, Bosch B-J, Beer M,**  
 435 **Müller MA, Kellam P, Drosten C.** 2014. Human Infection with MERS Coronavirus after  
 436 Exposure to Infected Camels, Saudi Arabia, 2013. *Emerg. Infect. Dis.* **20**:1012–5.
- 437 7. **Maged G. Hemida, Daniel K.W. Chu, Leo L.M. Poon, Ranawaka A.P.M. Perera,**  
 438 **Mohammad A. Alhammadi, Hoi-yee Ng, Lewis Y. Siu, Yi Guan, Abdelmohsen**  
 439 **Alnaeem and MP.** 2014. MERS Coronavirus in Dromedary Camel Herd, Saudi Arabia.  
 440 *Infect Dis.* June 16 2014. <http://dx.doi.org/10.3201/eid2007.140571>.
- 441 8. **Azhar EI, El-Kafrawy SA, Farraj SA, Hassan AM, Al-Saeed MS, Hashem AM, Madani**  
 442 **TA.** 2014. Evidence for Camel-to-Human Transmission of MERS Coronavirus. *N. Engl. J.*  
 443 *Med.* June 4, 2014. DOI: 10.1056/NEJMoa1401505
- 444 9. **Perera RA, Wang P, Gomaa MR, El-Shesheny R, Kandeil A, Bagato O, Siu LY,**  
 445 **Shehata MM, Kayed AS, Moatasim Y, Li M, Poon LL, Guan Y, Webby RJ, Ali MA,**  
 446 **Peiris JS, Kayali G.** 2013. Seroepidemiology for MERS coronavirus using

- 447 microneutralisation and pseudoparticle virus neutralisation assays reveal a high prevalence  
 448 of antibody in dromedary camels in Egypt, June 2013. *Euro Surveill.* Sep 5;18:pii=20574.
- 449 10. **Reusken CBEM, Haagmans BL, Müller MA, Gutierrez C, Godeke G-J, Meyer B, Muth**  
 450 **D, Raj VS, Smits-De Vries L, Corman VM, Drexler J-F, Smits SL, El Tahir YE, De**  
 451 **Sousa R, van Beek J, Nowotny N, van Maanen K, Hidalgo-Hermoso E, Bosch B-J,**  
 452 **Rottier P, Osterhaus A, Gortázar-Schmidt C, Drosten C, Koopmans MPG.** 2013.  
 453 Middle East respiratory syndrome coronavirus neutralising serum antibodies in dromedary  
 454 camels: a comparative serological study. *Lancet Infect. Dis.* 13:859–66.
- 455 11. **Memish ZA, Zumla AI, Al-Hakeem RF, Al-Rabeeah AA, Stephens GM.** 2013. Family  
 456 cluster of Middle East respiratory syndrome coronavirus infections. *N. Engl. J. Med.*  
 457 **368:**2487–94.
- 458 12. **Assiri A, McGeer A, Perl TM, Price CS, Al Rabeeah AA, Cummings DAT, Alabdullatif**  
 459 **ZN, Assad M, Almulhim A, Makhdoom H, Madani H, Alhakeem R, Al-Tawfiq JA,**  
 460 **Cotten M, Watson SJ, Kellam P, Zumla AI, Memish ZA.** 2013. Hospital outbreak of  
 461 Middle East respiratory syndrome coronavirus. *N. Engl. J. Med.* **369:**407–16.
- 462 13. **Cotten M, Watson SJ, Kellam P, Al-Rabeeah AA, Makhdoom HQ, Assiri A, Al-Tawfiq**  
 463 **JA, Alhakeem RF, Madani H, AlRabiah FA, Hajjar S Al, Al-nassir WN, Albarrak A,**  
 464 **Flemban H, Balkhy HH, Alsubaie S, Palser AL, Gall A, Bashford-Rogers R, Rambaut**  
 465 **A, Zumla AI, Memish ZA.** 2013. Transmission and evolution of the Middle East respiratory



- 466 syndrome coronavirus in Saudi Arabia: a descriptive genomic study. *Lancet*. **382**:  
 467 1993-2002.
- 468 14. **Ratia K, Pegan S, Takayama J, Sleeman K, Coughlin M, Baliji S, Chaudhuri R, Fu W,**  
 469 **Prabhakar BS, Johnson ME, Baker SC, Ghosh AK, Mesecar AD**. 2008. A noncovalent  
 470 class of papain-like protease/deubiquitinase inhibitors blocks SARS virus replication. *Proc.*  
 471 *Natl. Acad. Sci. U. S. A.* **105**:16119–16124.
- 472 15. **Lindner HA, Fotouhi-Ardakani N, Lytvyn V, Lachance P, Sulea T, Ménard R**. 2005. The  
 473 papain-like protease from the severe acute respiratory syndrome coronavirus is a  
 474 deubiquitinating enzyme. *J. Virol.* **79**:15199–208.
- 475 16. **Barretto N, Jukneliene D, Ratia K, Chen Z, Mesecar AD, Baker SC**. 2005. The  
 476 Papain-Like Protease of Severe Acute Respiratory Syndrome Coronavirus Has  
 477 Deubiquitinating Activity. *J Virol* **79**:15189–15198.
- 478 17. **Ratia K, Saikatendu KS, Santarsiero BD, Barretto N, Baker SC, Stevens RC, Mesecar**  
 479 **AD**. 2006. Severe acute respiratory syndrome coronavirus papain-like protease□:  
 480 Structure of a viral deubiquitinating enzyme. *Proc. Natl. Acad. Sci. U. S. A.* **103**:5717–22.
- 481 18. **Frieman M, Ratia K, Johnston RE, Mesecar AD, Baric RS**. 2009. Severe acute  
 482 respiratory syndrome coronavirus papain-like protease ubiquitin-like domain and catalytic  
 483 domain regulate antagonism of IRF3 and NF-kappaB signaling. *J. Virol.* **83**:6689–705.

- 484 19. **Clementz M, Chen Z, Banach BS, Wang Y, Sun L, Ratia K, Baez-Santos YM, Wang J,**  
 485 **Takayama J, Ghosh AK, Li K, Mesecar AD, Baker SC.** 2010. Deubiquitinating and  
 486 interferon antagonism activities of coronavirus papain-like proteases. *J. Virol.* **84**:4619–29.
- 487 20. **Ghosh AK, Takayama J, Rao KV, Ratia K, Chaudhuri R, Mulhearn DC, Lee H, Nichols**  
 488 **DB, Baliji S, Baker SC, Johnson ME, Mesecar AD.** 2010. Severe acute respiratory  
 489 syndrome coronavirus papain-like novel protease inhibitors: design, synthesis,  
 490 protein-ligand X-ray structure and biological evaluation. *J. Med. Chem.* **53**:4968–79.
- 491 21. **Roberts A, Deming D, Paddock CD, Cheng A, Yount B, Vogel L, Herman BD, Sheahan**  
 492 **T, Heise M, Genrich GL, Zaki SR, Baric R, Subbarao K.** 2007. A mouse-adapted  
 493 SARS-coronavirus causes disease and mortality in BALB/c mice. *PLoS Pathog.* **3**:e5.
- 494 22. **Day CW, Baric R, Cai SX, Frieman M, Kumaki Y, Morrey JD, Smee DF, Barnard DL.**  
 495 2009. A new mouse-adapted strain of SARS-CoV as a lethal model for evaluating antiviral  
 496 agents *in vitro* and *in vivo*. *Virology* **395**:210–22.
- 497 23. **McCray PB, Pewe L, Wohlford-Lenane C, Hickey M, Manzel L, Shi L, Netland J, Jia HP,**  
 498 **Halabi C, Sigmund CD, Meyerholz DK, Kirby P, Look DC, Perlman S.** 2007. Lethal  
 499 infection of K18-hACE2 mice infected with severe acute respiratory syndrome coronavirus.  
 500 *J. Virol.* **81**:813–21.

- 501 24. **Tseng C-TK, Huang C, Newman P, Wang N, Narayanan K, Watts DM, Makino S,**  
502 **Packard MM, Zaki SR, Chan T-S, Peters CJ.** 2007. Severe acute respiratory syndrome  
503 coronavirus infection of mice transgenic for the human Angiotensin-converting enzyme 2  
504 virus receptor. *J. Virol.* **81**:1162–73.
- 505 25. **Munster VJ, de Wit E, Feldmann H.** 2013. Pneumonia from human coronavirus in a  
506 macaque model. *N. Engl. J. Med.* **368**:1560–2.
- 507 26. **De Wit E, Rasmussen AL, Falzarano D, Bushmaker T, Feldmann F, Brining DL,**  
508 **Fischer ER, Martellaro C, Okumura A, Chang J, Scott D, Benecke AG, Katze MG,**  
509 **Feldmann H, Munster VJ.** 2013. Middle East respiratory syndrome coronavirus  
510 (MERS-CoV) causes transient lower respiratory tract infection in rhesus macaques. *Proc.*  
511 *Natl. Acad. Sci. U. S. A.* **110**:16598–16603.
- 512 27. **Coleman CM, Matthews KL, Goicochea L, Frieman MB.** 2013. Wild type and innate  
513 immune deficient mice are not susceptible to the Middle East Respiratory Syndrome  
514 Coronavirus. *J. Gen. Virol.* **95**(Pt 2):408-12
- 515 28. **De Wit E, Prescott J, Baseler L, Bushmaker T, Thomas T, Lackemeyer MG, Martellaro**  
516 **C, Milne-Price S, Haddock E, Haagmans BL, Feldmann H, Munster VJ.** 2013. The  
517 Middle East respiratory syndrome coronavirus (MERS-CoV) does not replicate in Syrian  
518 hamsters. *PLoS One* **8**:e69127.

- 519 29. **Raj VS, Mou H, Smits SL, Dekkers DHW, Müller MA, Dijkman R, Muth D, Demmers**  
520 **JAA, Zaki A, Fouchier RAM, Thiel V, Drosten C, Rottier PJM, Osterhaus ADME,**  
521 **Bosch BJ, Haagmans BL.** 2013. Dipeptidyl peptidase 4 is a functional receptor for the  
522 emerging human coronavirus-EMC. *Nature* **495**:251–4.
- 523 30. **Zhao J, Li K, Wohlford-Lenane C, Agnihothram SS, Fett C, Zhao J, Gale MJ, Baric RS,**  
524 **Enjuanes L, Gallagher T, McCray PB, Perlman S.** 2014. Rapid generation of a mouse  
525 model for Middle East respiratory syndrome. *Proc. Natl. Acad. Sci. U. S. A.* **111**:4970–5.
- 526 31. **Agnihothram S, Yount BL, Donaldson EF, Huynh J, Menachery VD, Gralinski LE,**  
527 **Graham RL, Becker MM, Tomar S, Scobey TD, Osswald HL, Whitmore A, Gopal R,**  
528 **Ghosh AK, Mesecar A, Zambon M, Heise M, Denison MR, Baric RS.** 2014. A mouse  
529 model for Betacoronavirus subgroup 2c using a bat coronavirus strain HKU5 variant. *MBio*  
530 **5**:e00047–14.
- 531 32. **Xiong C, Levis R, Shen P, Schlesinger S, Rice C, Huang H.** 1989. Sindbis virus: an  
532 efficient, broad host range vector for gene expression in animal cells. *Science.*  
533 **243**:1188–1191.
- 534 33. **Johnston C, Jiang W, Chu T, Levine B.** 2001. Identification of genes involved in the host  
535 response to neurovirulent alphavirus infection. *J. Virol.* **75**:10431–45.

- 536 34. **Levine B, Goldman JE, Jiang HH, Griffin DE, Hardwick JM.** 1996. Bc1-2 protects mice  
 537 against fatal alphavirus encephalitis. *Proc. Natl. Acad. Sci. U. S. A.* **93**:4810–5.
- 538 35. **Lenschow DJ, Giannakopoulos N V, Gunn LJ, Johnston C, Guin AKO, Schmidt RE,**  
 539 **Levine B, Iv HWV.** 2005. Identification of Interferon-Stimulated Gene 15 as an Antiviral  
 540 Molecule during Sindbis Virus Infection *In Vivo*. *J. Virol.* **79**:13974–13983.
- 541 36. **Frias-Staheli N, Giannakopoulos N V, Kikkert M, Taylor SL, Bridgen A, Paragas J,**  
 542 **Richt J a, Rowland RR, Schmaljohn CS, Lenschow DJ, Snijder EJ, Garcia-Sastre A,**  
 543 **Virgin HW.** 2007. Ovarian tumor domain-containing viral proteases evade ubiquitin- and  
 544 ISG15-dependent innate immune responses. *Cell Host Microbe* **2**:404–16.
- 545 37. **Nicholson B, Leach CA, Goldenberg SJ, Francis DM, Kodrasov MP, Tian X, Shanks J,**  
 546 **Sterner DE, Bernal A, Mattern MR, Wilkinson KD, Butt TR.** 2008. Characterization of  
 547 ubiquitin and ubiquitin-like-protein isopeptidase activities. *Protein Sci.* **17**:1035–43.
- 548 38. **Kilianski A, Mielech A, Deng X, Baker SC.** 2013. Assessing Activity and Inhibition of  
 549 MERS-CoV Papain-like and 3C-like Proteases Using Luciferase-based Biosensors. *J. Virol.*  
 550 **87**:11955–11962.
- 551 39. **Baez-Santos YM, Barraza SJ, Wilson MW, Agius M, Mielech AM, Davis NM, Baker SC,**  
 552 **Larsen SD, Mesecar AD.** 2014. X-Ray Structural and Biological Evaluation of a Series of

- 553 Potent and Highly Selective Inhibitors of Human Coronavirus Papain-Like Proteases. *J.*  
 554 *Med. Chem.* **57**:2393–2412
- 555 40. **Skaug B, Chen ZJ.** 2010. Emerging role of ISG15 in antiviral immunity. *Cell* **143**:187–190.
- 556 41. **Lenschow DJ, Lai C, Frias-staheli N, Giannakopoulos N V, Lutz A, Wolff T, Osiak A,**  
 557 **Levine B, Schmidt RE, Garcı A, Leib DA, Pekosz A, Knobeloch K, Horak I, Whiting H,**  
 558 **Iv V.** 2007. IFN-stimulated gene 15 functions as a critical antiviral molecule against  
 559 influenza, herpes, and Sindbis viruses. *Proc Natl Acad Sci USA* **104**:1371–1376.
- 560 42. **Ma X-Z, Bartczak A, Zhang J, He W, Shalev I, Smil D, Chen L, Phillips J, Feld JJ,**  
 561 **Selzner N, Levy G, McGilvray I.** 2014. Protein interferon-stimulated gene 15 conjugation  
 562 delays but does not overcome coronavirus proliferation in a model of fulminant hepatitis. *J.*  
 563 *Viro.* **88**:6195–204.
- 564 43. **Cong X-L, Lo M-C, Reuter BA, Yan M, Fan J-B, Zhang D-E.** 2012. Usp18 promotes  
 565 conventional CD11b+ dendritic cell development. *J. Immunol.* **188**:4776–81.
- 566 44. **Lu G, Hu Y, Wang Q, Qi J, Gao F, Li Y, Zhang Y, Zhang W, Yuan Y, Bao J, Zhang B,**  
 567 **Shi Y, Yan J, Gao GF.** 2013. Molecular basis of binding between novel human coronavirus  
 568 MERS-CoV and its receptor CD26. *Nature* **500**:227–31.

- 569 45. **Chen Y, Rajashankar KR, Yang Y, Agnihothram SS, Liu C, Lin Y-L, Baric RS, Li F.**  
570 2013. Crystal structure of the receptor-binding domain from newly emerged Middle East  
571 respiratory syndrome coronavirus. *J. Virol.* **87**:10777–83.
- 572 46. **Fouchier RAM, Hartwig NG, Bestebroer TM, Niemeyer B, de Jong JC, Simon JH,**  
573 **Osterhaus ADME.** 2004. A previously undescribed coronavirus associated with respiratory  
574 disease in humans. *Proc. Natl. Acad. Sci. U. S. A.* **101**:6212–6.
- 575 47. **Van der Hoek L, Pyrc K, Jebbink MF, Vermeulen-Oost W, Berkhout RJM, Wolthers**  
576 **KC, Wertheim-van Dillen PME, Kaandorp J, Spaargaren J, Berkhout B.** 2004.  
577 Identification of a new human coronavirus. *Nat. Med.* **10**:368–73.
- 578 48. **Woo PCY, Lau SKP, Chu C, Chan K, Tsoi H, Huang Y, Wong BHL, Poon RWS, Cai JJ,**  
579 **Luk W, Poon LLM, Wong SSY, Guan Y, Peiris JSM, Yuen K.** 2005. Characterization and  
580 complete genome sequence of a novel coronavirus, coronavirus HKU1, from patients with  
581 pneumonia. *J. Virol.* **79**:884–95.
- 582
- 583

584 **Figure Legends**

585 **Figure 1. Generation of chimeric SIP viruses.** (A) Schematic diagram of chimeric Sindbis  
586 viruses expressing ISG15, HCV-IRES and SARS-CoV PLpro or MERS-CoV PLpro . (B)  
587 Detection of PLpro and ISG15 from cells infected with SIP viruses. BHK-21 cells were mock  
588 infected or infected with SIP viruses as indicated at moi of 5, lysates prepared at 18 hrs  
589 post-infection, and proteins detected by immunoblotting. (C) Replication kinetics of SIP  
590 viruses. BHK-21 cells were infected SIP viruses as indicated at moi of 5 and supernatants  
591 were collected at indicated time points. Viral titer was representative of three independent  
592 experiments. Error bars represent SD.

593 **Figure 2. PLpros expressed by chimeric Sindbis virus have delISGylating activity.**  
594 BHK-21 cells were transfected with ISGylating machinery expression plasmids (myc-ISG15,  
595 Ube1L, Ubch8, and Herc5) and subsequently infected with SIP viruses as indicated. Cells  
596 lysate were probed with anti-myc to detect ISGylated proteins and unconjugated ISG15. The  
597 expression of PLpro and beta-actin as a loading control were detected with anti-V5 and  
598 anti-beta actin antibodies, respectively.

599 **Figure 3. PLpros inhibit the ISG15-mediated antiviral effect in IFNAR<sup>-/-</sup> mice.** Seven to  
600 eight-week old male IFNAR<sup>-/-</sup> mice were injected in footpad with the WT ( SWT or MWT) or  
601 MT ( SMT or MMT) SIP viruses at  $6 \times 10^6$  PFU and monitored for weight loss. Data are pooled  
602 from three independent experiments. Numbers of mice per group are indicated in parenthesis.



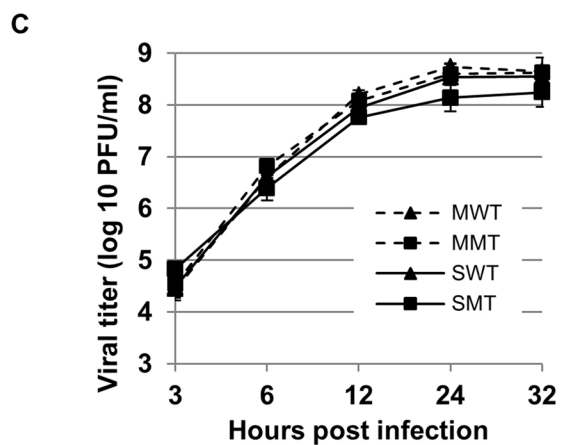
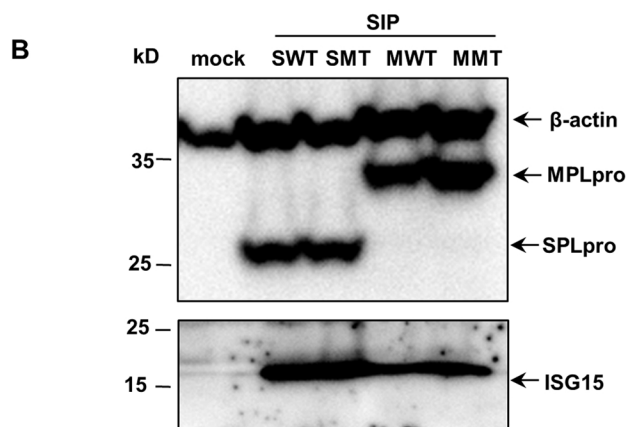
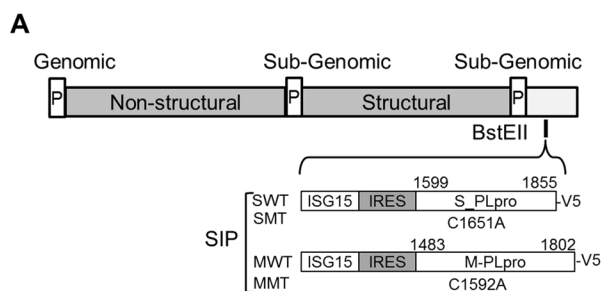
603 The statistical differences in body weight loss (A) and survival rate (B) were analyzed by  
604 Prism software with the two-way ANOVA test and the log-rank test, respectively. Error bars  
605 represent SEM. \*,  $p < 0.05$ ; \*\*,  $p < 0.01$ ; \*\*\*,  $p < 0.001$ .

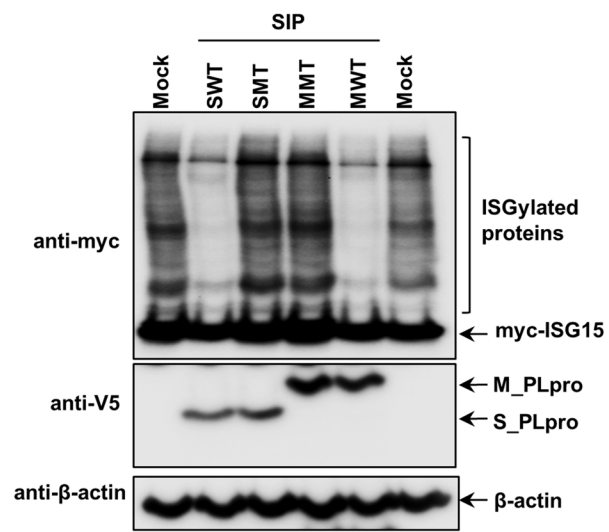
606 **Figure 4. Compound 3e blocks the deISGylating activity of SARS-CoV PLpro in cell**  
607 **culture.** (A) The structures of tested compounds. (B) BHK-21 cells were transfected with  
608 ISGylating machinery plasmids and subsequently infected with SIP-SWT virus as indicated  
609 followed by addition of 50  $\mu\text{M}$  compound 3e or 3h; (C) BHK-21 cells co-transfected with  
610 ISGylating machinery plasmids and USP18 expression plasmids were treated with 50  $\mu\text{M}$   
611 compound 3e or DMSO. Cell lysates were immunoblotted with anti-myc antibody for detecting  
612 the ISGylated proteins. Expressions of PLpro, USP18, and beta-actin as loading control were  
613 detected with anti-V5, anti-HA, and anti-beta actin antibodies, respectively.

614 **Figure 5. Compound 3e blocks PLpro from disrupting ISG15-mediated protection in**  
615 **IFNAR<sup>-/-</sup> mice.** IFNAR<sup>-/-</sup> mice were infected subcutaneously with SIP-SWT virus at 0 d.p.i and  
616 administered i.p. 50  $\mu\text{g}$  per mouse of compound 3e or vehicle only at 0 and 2 d.p.i. Mice  
617 were monitored for body weight loss (A) and survival (B). Data are pooled from three  
618 independent experiments. Total mouse number per group indicated in parenthesis. The  
619 statistical differences in weight loss and survival were analyzed by Prism software using the 2  
620 way ANOVA test and the log-rank test, respectively. Error bars represent SEM. \*\*,  $p < 0.01$ .

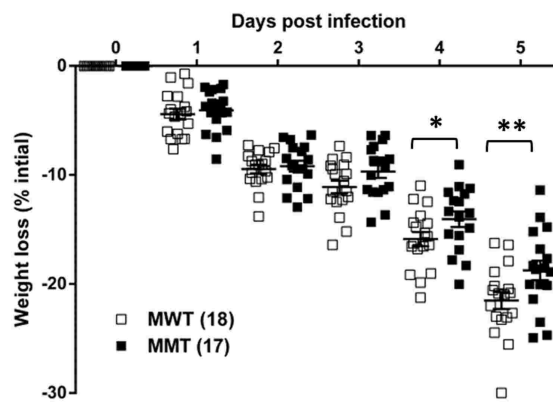
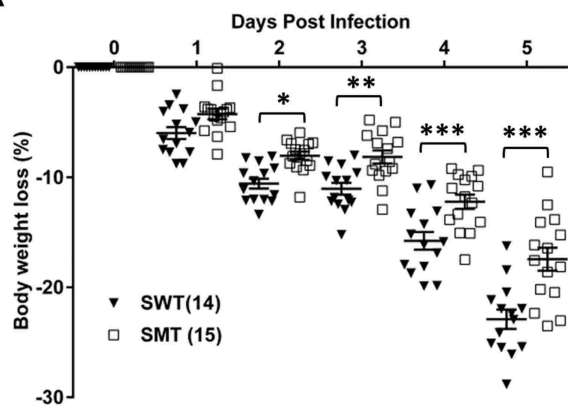
621 **Figure 6. Evaluation of PLpro inhibitor 3e in SARS-CoV MA15 mouse model.** (A) Five  
622 eight-week old Balb/c mice of each group were administered either i.n. a single dose of 20 µg  
623 Poly (I:C), or i.p. 50 µg per dose of 3e or vehicle at 4 hrs prior to infection i.n. with MA15 strain  
624 virus  $2 \times 10^4$  PFU. Infected mice were further treated with 3e or vehicle for twice a day at 0, 1,  
625 and 2 d.p.i. Mice were monitored for weight loss and mortality. (B) Viral titer in lung was  
626 determined at 4 d.p.i. The statistical differences in weight loss and titer were analyzed by  
627 Prism software using the T-test. Error bars represent SEM.

628

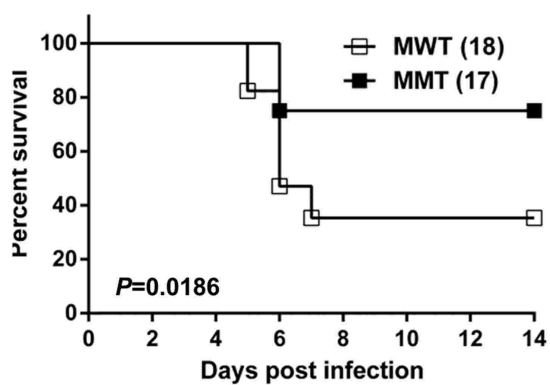
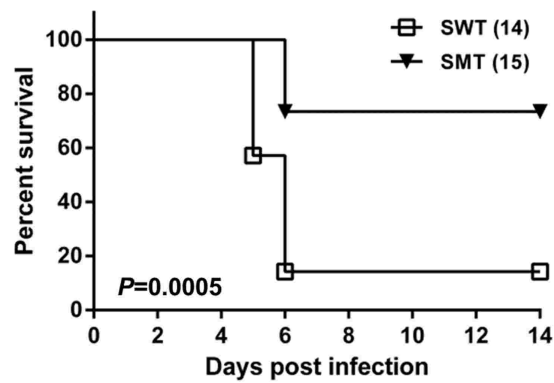


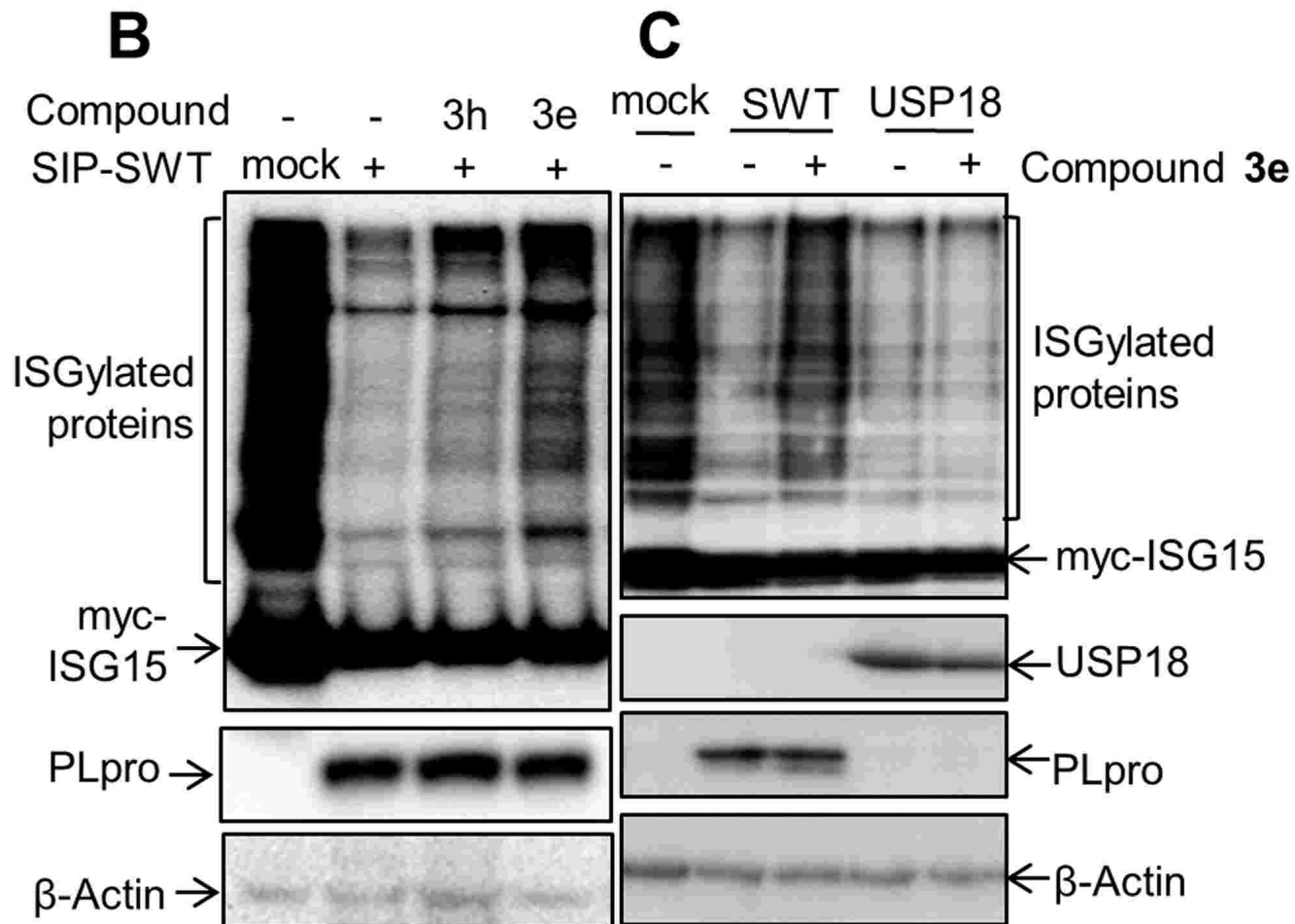
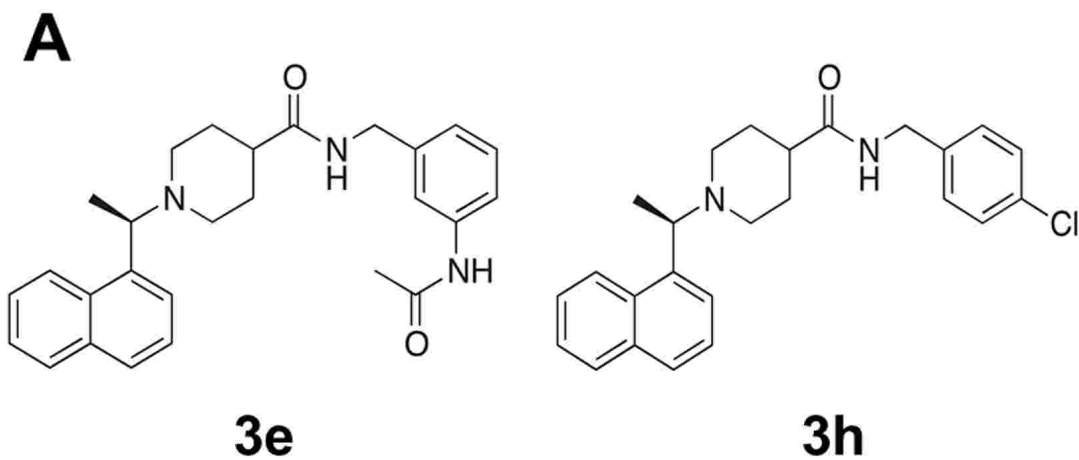


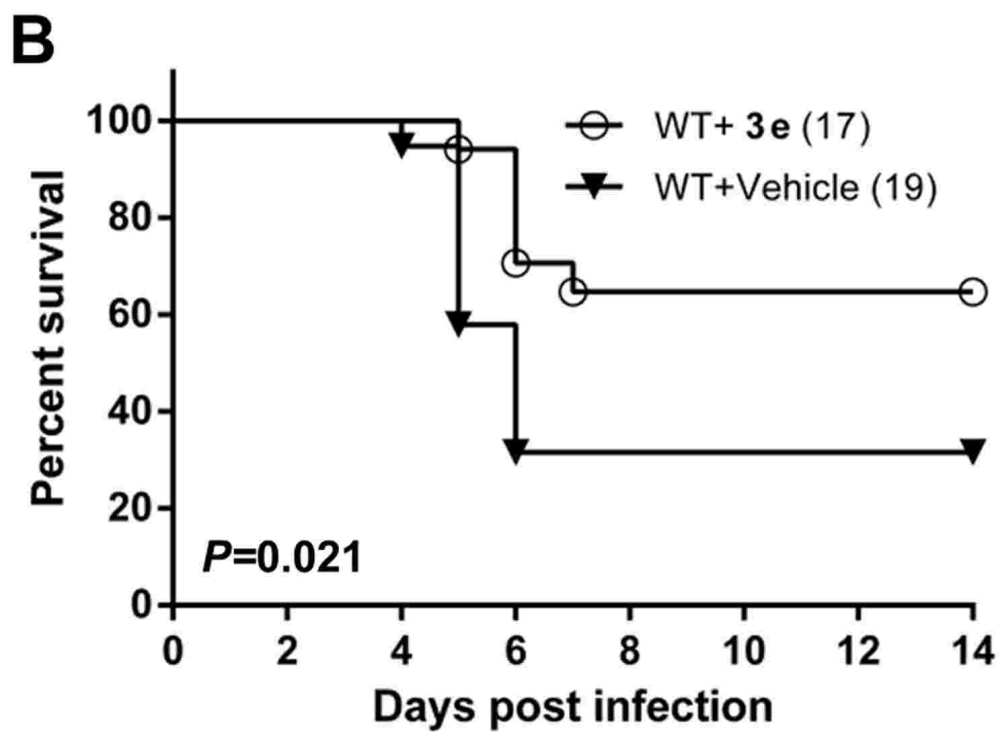
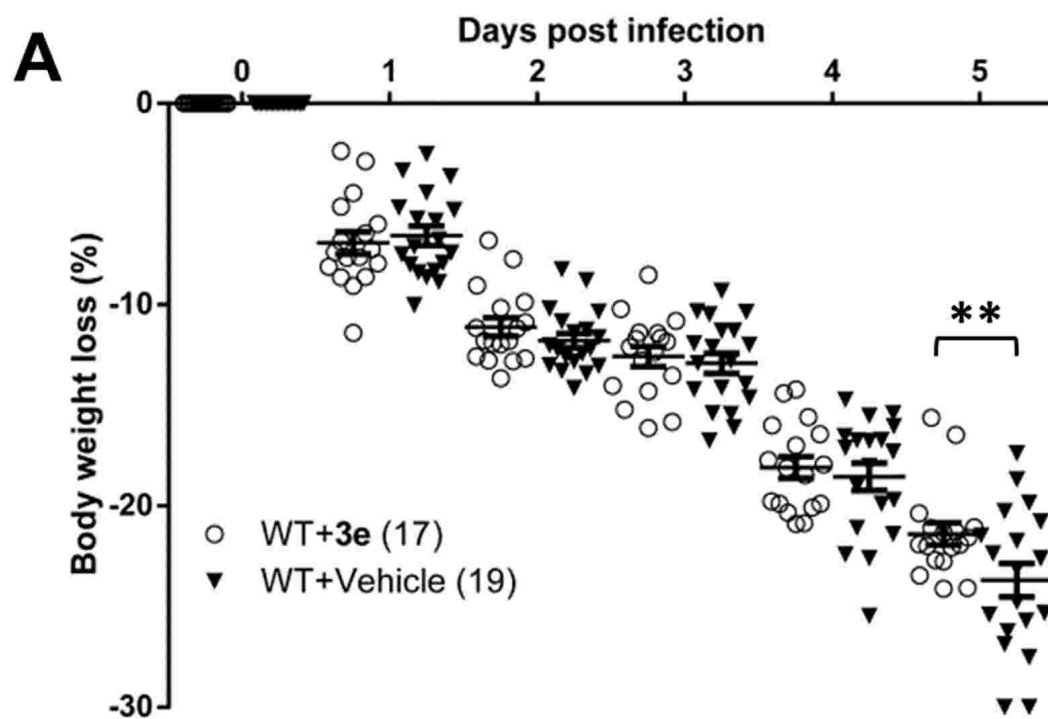
**A**



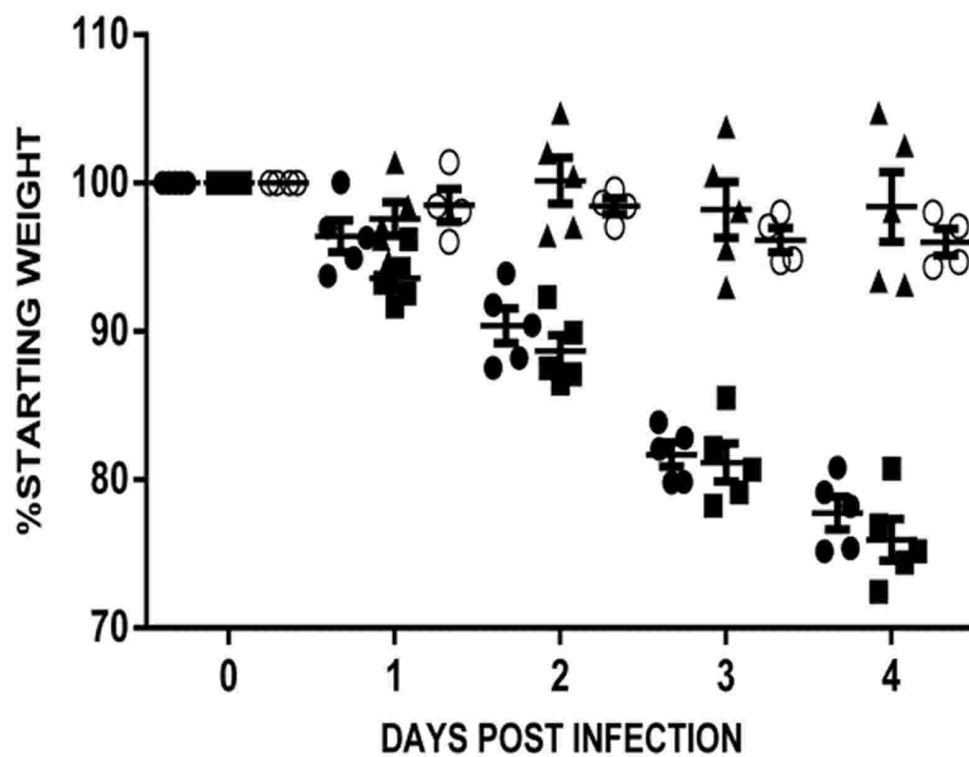
**B**







A



● 3e+MA15      ▲ 3e only  
 ■ Vehicle+ MA15      ○ Poly IC

B

